Twisted Solar Active Region Magnetic Fields as Drivers of Space Weather: Observational and Theoretical Investigations

Dibyendu Nandy [a,*], Duncan H. Mackay [b],
Richard C. Canfield [a] and P.C.H. Martens [a]

[a]*Department of Physics, Montana State University, Bozeman, MT 59717, USA*

[b]*School of Mathematics and Statistics, University of St. Andrews, St. Andrews, Fife, Scotland KY16 9SS, UK*

Abstract

The properties and dynamics of magnetic fields on the Sun's photosphere and outer layers – notably those within solar active regions – govern the eruptive activity of the Sun. These photospheric magnetic fields also act as the evolving lower boundary of the Sun-Earth coupled system. Quantifying the physical attributes of these magnetic fields and exploring the mechanisms underlying their influence on the near-Earth space environment are of vital importance for forecasting and mitigating adverse space weather effects. In this context, we discuss here a novel technique for measuring twist in the magnetic field lines of solar active regions that does not invoke the force-free field assumption. Twist in solar active regions can play an important role in flaring activity and the initiation of CMEs via the kink instability mechanism; we outline a procedure for determining this solar active region eruptive potential. We also discuss how twist in active region magnetic fields can be used as inputs in simulations of the coronal and heliospheric fields; specifically, we explore through simulations, the formation, evolution and ejection of magnetic flux ropes that originate in twisted magnetic structures. The results and ideas presented here are relevant for exploring the role of twisted solar active region magnetic fields and flux ropes as drivers of space weather in the Sun-Earth system.

Key words:
Solar Magnetic fields, Active Regions, Space Weather, Helicity, Flares, CMEs

* Corresponding author email: nandi@mithra.physics.montana.edu

1 Introduction

Twisted magnetic fields within solar active regions (ARs) indicate the presence of stressed non-potential flux systems that are highly eruptive (Canfield, McKenzie & Hudson, 1999; Sammis, Tang & Zirin, 2000; Schrijver et al., 2005). They are believed to be at the heart of many energetic solar phenomena which govern the Sun-Earth system. Twist is a component of magnetic helicity that describes how magnetic field lines wind about the axis of a flux tube; it is an important indicator of the topology or morphology of the 3-D magnetic structure underlying AR loops observed in the solar atmosphere and is known to play an important role in flaring activity (Nandy et al., 2003; Hahn et al., 2005). Photospheric AR twists are used as inputs to model coronal magnetic structures, study their energetics and compare the reconstructed magnetic topology to space observations (Valori, Kliem & Keppens, 2005; Régnier & Canfield, 2006). Twist also plays a role in MHD modelling of the evolution of coronal and heliospheric magnetic fields (Amari et al. 2003; Mackay & van Ballegooijen, 2006), including simulations of large-scale eruptions such as coronal mass ejections (CMEs) mediated via the kink instability mechanism (Fan 2005).

The aim of this paper is twofold. The first is to outline a new observational technique that we are developing for the measurement of twist in the flux systems of solar ARs from photospheric vector magnetograms and to quantify the susceptibility of these flux systems to the MHD kink instability mechanism that may result in solar eruptive events (Section 2). The second is to show, using numerical magnetohydrodynamic (MHD) simulations, how magnetic flux ropes that underlie solar energetic events such as Coronal Mass Ejections (CMEs) originate and evolve from these twisted magnetic structures (Section 3). We also discuss in Section 4, the importance of such studies in the context of understanding and predicting the influence of the Sun on our space environment.

2 Observational Investigations: Quantifying Active Region Twist and Eruptive Potential

We begin with the motivation behind the development of a new technique for measuring solar photospheric AR twist. To date, the most widely used method for inferring the twist of solar ARs has been the determination of the value of the force-free field parameter α in the force-free field equation

$$\nabla \times \mathbf{B} = \alpha \mathbf{B} \tag{1}$$

that best fits the observed horizontal magnetic fields of an active region, called α_{best} (Pevtsov, Canfield & Metcalf, 1995). The α_{best} method assumes that the force-free-field equation (above) is applicable to photospheric AR magnetic fields, and that the latter is characterized by a single (constant) value of the force-free field parameter α in Equation 1. However, the photosphere is a forced layer with the plasma-β parameter (ratio of gas to magnetic pressure) close to unity (Metcalf et al. 1995). It has been claimed that the use of α_{best} underestimates the amount of actual twist present (Leka, Fan & Barnes, 2005; Valori, Kliem, & Keppens, 2005). Accurate quantitative measurements are needed to test observationally whether MHD kinking indeed is the trigger for CMEs and eruptive flares (for conflicting viewpoints, see Leamon et al., 2003 and Leka, Fan & Barnes, 2005), for use as inputs in reliable reconstructions and modelling of coronal and heliospheric magnetic fields and understanding sub-photospheric flux tube dynamics (see Nandy, 2006). We have developed a flux-tube fitting technique for measurement of photospheric AR twist that is based on theoretical and numerical studies and which does not rely on the force-free assumption (Equation 1). We describe this below.

In the literature, various descriptors of twist are used, including the *total twist* T of a magnetic loop of length L between footpoints, and the *twist density* (i.e., twist per unit length) q. These two quantities are related through the following equation

$$T = qL \tag{2}$$

where $T/2\pi$ is the *number* of winds about the axis over the length L. If $T = 2\pi$, the field lines wind exactly once over the length L. Henceforth, we refer to the twist density q simply as "twist".

We determine q from photospheric vector magnetograms under the assumption that the underlying AR magnetic field structure can be represented by a cylindrical flux tube (or flux rope) – an approach that is supported by theory, simulations and observational constraints on flux tube dynamics in the SCZ (Fan, Fisher & McClymont, 1994; Fisher, Fan & Howard, 1995). A cylindrical flux tube is characterized by its three magnetic field components, namely, B_r, B_θ and B_z. Twisting a flux tube uniformly by a quantity q just changes the azimuthal field $B_\theta(r)$ such that $B_\theta(r) = qrB_z(r)$, where B_z is the axial field. Under the assumption of this uniformly twisted flux tube, it follows then that the quantity we want to extract is

$$q = \frac{B_\theta(r)}{rB_z(r)}. \tag{3}$$

Since leading (Hale) polarities of solar ARs are more coherent and representative of the underlying cylindrical geometry (Fan, Fisher & DeLuca 1993),

we use vector magnetograms of the leading polarities of ARs for this analysis. Vector magnetograms are routinely used to infer B_x, B_y and B_z components of the magnetic field in the local heliographic Cartesian-coordinate system in each magnetogram pixel, following methods described by, e.g., Canfield et al. (1993). Once we have identified the leading polarity of a given AR, we first determine the flux-weighted-centroid (FWC) of this flux system assuming cylindrical symmetry and then through a coordinate transformation, extract the three components of the underlying cylindrical structure, B_r, B_θ and B_z along with the radial distance r of each of these measurements from the origin (FWC). In Figure 1 we show a vector magnetogram from the Haleakala Stokes Polarimeter (HSP, Mickey, 1985) that includes the leading positive polarity of AR 7289 (classified as a Mt. Wilson β-region, having a simple bipolar structure) and show its inferred FWC.

The final step involves the determination of q as given by the relationship in Equation 3 using the radial distance r and the corresponding B_θ and B_z values. The overall twist characterizing the AR is determined by calculating the linear best-fit slope of the B_θ/B_z versus radial distance r distribution – a quantity that we define as q_{fit}. Figure 2 (left) shows the determination of q_{fit} from the B_θ/B_z data for AR 7289. The recovered best-fit twist for AR 7289 from this flux-tube fitting technique is $q_{fit} = -4.89 \times 10^{-8}$ m^{-1}.

We now outline a methodology for the extraction of another quantity defining AR flux ropes – the critical twist value q_{crit} that is necessary for determining their susceptibility to the kink instability mechanism (conversion of twist to writhe and deformation of the flux-tube axis itself) that is thought to trigger breakout reconnection in CMEs (Fan, 2005) and kink flux ropes in the SCZ (Linton, Longcope & Fisher, 1996; Linton et al. 1999). Accurate quantitative measurements are important. While some studies indicate that a total twist of $T = qL = 2\pi$ is sufficient for flux tubes to be kink unstable (Priest, 1982 Fan & Gibson, 2004), other studies point out that the critical total twist can be as high as 4.8π (Mikić, Schnack & Van Hoven, 1990); the differences arise from assumptions regarding various flux tube models. Our new methodology is model-independent and is motivated from the the analysis and numerical simulations of Linton, Longcope & Fisher (1996) and Linton et al. (1999). Their instability analysis and extensive numerical simulations show that the critical twist threshold for the cylindrical flux tube to be susceptible to the kink instability, q_{crit}, is related to the coefficient (μ) of the r^2 term in the Taylor series expansion of the axial field $B_z = B_0(1 - \mu r^2 - p r^4 - ...)$, where we've folded R^{-2} into μ, R^{-4} into p, etc (here, B_0 is the field strength at the axis, i.e., at $r = 0$ and R is the radius of the tube). If one considers a lowest-order appropriate truncation then this simplifies to

$$B_z = B_0 \left(1 - \mu r^2\right). \tag{4}$$

These theoretical and numerical flux tube dynamics studies show that the critical twist is simply $q_{crit} = \mu^{1/2}$; if the twist q of the flux tube exceeds the threshold q_{crit} then the flux tube is kink unstable (Linton, Longcope & Fisher, 1996; Linton et al. 1999). Our aim is to measure q_{crit} from vector magnetograms and thus quantify observationally whether a given AR is susceptible to kink instability. To determine the critical twist we follow the theoretical considerations above and fit an equation of the form of Equation 4 to the radial profile of B_z for AR 7289. To rule out the influence of ephemeral regions and noise, only pixels with $B_z > 300$ G are considered. For AR 7289, the fit shown in Figure 2 (right) gives us $B_0 = 1436$ G and critical twist $q_{crit} = \mu^{1/2} = 7.27 \times 10^{-8}$ m^{-1}.

Whether the coronal magnetic field structure associated with a twisted AR is kink unstable and likely to erupt depends additionally on line-tying considerations – specifically on the total twist T in the coronal loop-length that is line-tied between two photospheric footpoints rooted within the two polarities of the AR (see e.g., Hood & Priest, 1979; Einaudi & van Hoven, 1983; Melville, Hood & Priest, 1986; Török, Kliem & Titov, 2004). In this case, the coronal loops are unstable to helical kink perturbations with wavelengths below $2\pi/q_{crit}$ (equivalently, coronal loop-lengths exceeding this wavelength are kink-unstable). As discussed in these papers, the critical (total) twist T_{crit} is at least 2π; it is often higher due to line-tying conditions, and the exact value depends on the assumed field structure and equilibrium configuration (Hood & Priest, 1979; Einaudi & van Hoven, 1983; Melville, Hood & Priest, 1986; Török, Kliem & Titov, 2004). Therefore, for determining the stability of coronal loops associated with a twisted AR, one needs to estimate the total twist $T = qL$, where L is the coronal loop length and q is the twist of the AR flux tube. Note also that an AR flux system with twist exceeding q_{crit} is an inherently unstable structure, and will quickly trade some of its twist for writhe through kink instability. Therefore, it is unlikely that many observed AR structures will have twist exceeding q_{crit}, unless it is observed during the early phase of its emergence process.

3 Theoretical Investigations: Simulations of Flux Rope Formation, Evolution and Ejection

In the solar atmosphere, magnetic fields produce a wide variety of phenomena. These phenomena include, sigmoids (Rust & Kumar, 1996; Canfield et al., 1999; Pevtsov, 2002), solar filaments (Priest, 1989; Martin, 1998), solar flares (Priest, 1982; Somov, 1992) and coronal mass ejections (Hundhausen, 1993; Low, 2001). A common feature of these phenomena is that they require the presence of highly sheared or twisted magnetic fields called magnetic flux ropes (Russell et al., 1990; Amari et al., 1999; Low, 2001). Flux ropes may be stable

for many days, then suddenly loose equilibrium (Torok & Kleim, 2005; Amari et al, 2003; Lin & Forbes, 2000 ; Isenberg et al., 1993), resulting in a flare, filament eruption or coronal mass ejection. To understand what causes such eruptions we need to determine how flux ropes are related to the magnetic helicity of active regions. In this section idealized simulations are carried out of the interaction of two bipolar regions (Mackay and van Ballegooijen, 2005, Mackay et al., 1997) to determine the relationship between the helicity in active regions and how flux ropes form and are ejected from the solar corona.

To consider the formation of magnetic flux ropes we use a magnetic flux transport and magnetofrictional model (van Ballegooijen, Priest and Mackay, 2000, Mackay and van Ballegooijen, 2001, Mackay and van Ballegooijen, 2006a,b). The Sun's magnetic field, $\mathbf{B}(= B_r, B_\theta, B_\phi) = \nabla \times \mathbf{A}$ is evolved by the induction equation. At the lower boundary, the photosphere, the magnetic field is driven by the large-scale flows of differential rotation, meridional flows and surface diffusion, the later representing the effect of small-scale flows such as supergranulation (Leighton, 1964). To represent these physical processes appropriate boundary conditions are applied at the lower boundary (for details, see Mackay and van Ballegooijen, 2006 a,b). In the coronal region the magnetic field evolves in response to these motions through the non-ideal induction equation,

$$\frac{\partial \mathbf{A}}{\partial t} = \mathbf{v} \times \mathbf{B} - \eta_c \mathbf{j}, \tag{5}$$

where $\mathbf{v}(\mathbf{r}, t)$ is the plasma velocity, $\mathbf{j} = \nabla \times \mathbf{B}$ and η_c the coronal diffusion. To ensure that the coronal field evolves through a series of force-free states a magneto-frictional method is employed (Yang et al., 1986). We assume that the coronal plasma velocity is given by,

$$\mathbf{v} = \frac{1}{\nu} \frac{\mathbf{j} \times \mathbf{B}}{B^2} + v_o e^{-(2.5R_\odot - r)/r_w} \hat{\mathbf{r}}.$$

where the first term on the right hand side represents in an approximate manner the fact that the Lorentz force is dominant in the corona. The second term represents a radial outflow velocity which is imposed to ensure that the field lines remain radial at the source surface ($r = 2.5R_\odot$). Full details of the choice of these parameters along with the numerical scheme applied can be found in Mackay and van Ballegooijen (2006a,b).

In Figure 3, the initial relaxed equilibrium configuration can be seen. To produce this configuration, two bipoles expressed by the mathematical form,

$$B_x = B_0 e^{0.5} \left(\frac{z}{\rho_0} e^{-\xi} + 4\beta \frac{xy}{\rho_0^2} e^{-2\xi} \right),$$

$$B_y = 2\beta B_0 e^{0.5} \left(1 - \frac{x^2 + z^2}{\rho_0^2} \right) e^{-2\xi},$$

$$B_z = B_0 e^{0.5} \left(-\frac{x}{\rho_0} e^{-\xi} + 4\beta \frac{yz}{\rho_0^2} e^{-2\xi} \right),$$

relative to their center point (ϕ_0, λ_0) are inserted, where $\xi \equiv [(x^2 + z^2)/2 + y^2]/\rho_0^2$, ρ_0 is the half separation between the peaks of the photospheric flux pattern (corresponding to a heliocentric angle of 5°), B_0 is the peak flux density ($B_0 = -200$ G), and β is a dimensionless parameter describing the twist of the magnetic field (in this form, the spherical coordinate system is transformed such that $x = \phi$, $y = -ln(tan(\theta/2))$, $z = ln(r/R_o dot)$). The bipoles are inserted in non-equilibrium over a finite region in the photosphere and corona. One is placed at $\phi_0 = 42°$, $\lambda_0 = 17°$ and the other at $\phi_0 = 65°$, $\lambda_0 = 17°$ where both are given the twist value of $\beta = -0.2$. Once inserted the bipoles expand to fill the entire coronal volume and relax to an equilibrium as shown in Figure 3 where the grayscale image shows the distribution of the radial magnetic field at the photosphere. White represents positive flux and black negative flux. The lines connecting the white and black regions represent coronal field lines where both bipoles have the same shear. In the papers of Mackay and van Ballegooijen (2006a,b) another example is considered where the trailing bipole (in the direction of rotation) has slightly more shear applied compared to the lead bipole.

Flux transport effects are then allowed to act on the magnetic field for a period of 45 days and the formation of flux ropes over the internal PIL of each bipole and external PIL between the bipoles occurs. The key physical effect that leads to the formation of the flux ropes is the surface diffusion of the flux. This process, described in terms of the large-scale supergranular diffusion first leads to the transport of sheared field lines to the PIL. Once there, cancellation of the opposite polarity foot points of the field lines and subsequent reconnection of them can produce an axial field component along the PIL. Examples of these highly sheared regions can be seen in Figure 4 where they are shown for (a) the two internal PILs on day 20 and (b) the external PIL between the bipoles on day 45. For the internal PILs strongly sheared inverse-S shaped (sigmoidal) structures – which are known to be associated with CMEs (Canfield, Hudson & McKenzie, 1999) – are found to lie above the internal PILs of both bipoles. In contrast to this, above the external PIL a much less twisted structure is found.

The larger the magnitude of the initial twist in the bipoles, the earlier in the simulation the flux ropes form. Although this is true for both the internal and external PIL's, the internal PILs show a much stronger variation. This

is because for the flux ropes to form above the external PILs, untwisted field lines lying in the outer extents of the bipoles have to be cancelled first, before the formation can start (for an extended discussion, see Mackay and van Ballegooijen, 2006a). This essentially takes the same amount of time irrespective of the magnitude of twist added to the internal parts of the bipole. In all of the simulations flux ropes may be formed by the combined effects of surface diffusion and differential rotation. The role of the initial twist is to affect the time it takes for flux ropes to form.

A surprising feature of the simulations is that once formed the flux ropes may then be expelled out of the computational box. This process is driven by the magnetic pressure force pinching and reconnecting field lines underneath the flux ropes as they rise. During this process the coronal field diverges from an equilibrium between the surface shearing motions and the relaxation. However once the flux ropes have been expelled such a balance is obtained once again. When the bipoles are given the same initial twist the flux ropes that form above the internal PILs are ejected at the same time. In Figure 5 an overview of the simultaneous ejection of the flux ropes can be seen. In Figure 5(a) the field lines can be seen on day 20 before the ejection begins. Above each of the bipoles a strongly sheared axis of the flux rope lies at low heights with weakly sheared arcades lying above it. In contrast, in Figure 5(b) (day 30) the axis of both flux ropes has risen by pushing the arcades above them upward. As each rises, a quasi-separatrix layer (QSL, Priest and Demoulin, 1995) forms underneath, through the distortion of the coronal field along its entire length in the corona. At this location, oppositely orientated field lines reconnect and the reconnected field lines help to push the axis of the flux rope further upwards. As the two flux ropes rise, they interact with one-another before they are ejected out of the top of the box. In contrast, in Mackay and van Ballegooijen (2006) – where the bipoles have different initial twists, the flux ropes are ejected at different times.

4   Conclusions

We have outlined novel observational techniques for measuring the twist of solar ARs from photospheric vector magnetograms and determining their susceptibility to the MHD kink instability. Using these techniques, it would be possible to quantify the eruptive potential of solar ARs – via the kink instability mechanism – that may result in eruptive flares or CMEs. Thus, this could be a basis for short-term (on the order of days) space weather forecasting based on photospheric vector magnetic field properties derived from magnetogram observations alone.

We have also shown through simulations how flux ropes may originate and

evolve into twisted magnetic structures through the combined action of surface flux transport processes (such as diffusion, meridional circulation and differential rotation) and how these flux ropes are subsequently ejected. The two bipole interactions described here, which is the simplest case, will describe the basic interactions occurring for many bipoles in more complicated (future) full-Sun simulations. We are currently developing techniques to utilize direct observational inputs of the twist component of magnetic helicity in solar ARs (as outlined in Section 2) to drive the photospheric and coronal field evolution simulations (as outlined in Section 3) to understand the magnetic topologies that spawn large-scale solar eruptions such as CMEs. Complementary to the earlier short-term space weather forecasting (on the order of days) based on magnetic field observations alone, these simulations can lead to long-term space weather forecasting (on the order of months) because of the cumulative effect of relatively slower photospheric magnetic field dynamics – which drives the formation and evolution of flux ropes.

References

[1] Amari, T., Luciani, J. F., Mikic, Z., Linker, J., 1999. Three-dimensional solutions of magnetohydrodynamic equations for prominence magnetic support: twisted magnetic flux rope. ApJL 518, L57–L60.

[2] Amari, T., Luciani, J. F., Aly, J. J., Mikic, Z., Linker, J., 2003. Coronal mass ejection: initiation, magnetic helicity, and flux ropes. II. Turbulent diffusion-driven evolution. ApJ 595, 1231–1250.

[3] Canfield, R.C., et al., 1993. The morphology of flare phenomena, magnetic fields, and electric currents in active regions. I - Introduction and methods. ApJ 411, 362–369.

[4] Canfield, R. C., Hudson, H. S., McKenzie, D. E., 1999. Sigmoidal morphology and eruptive solar activity. Geophysical Research Letters 26, 627–630.

[5] Fan, Y., 2005. Coronal mass ejections as loss of confinement of kinked magnetic flux ropes. ApJ 630, 543–551.

[6] Fan, Y., Fisher, G. H., DeLuca, E. E., 1993. The origin of morphological asymmetries in bipolar active regions. ApJ 405, 390–401.

[7] Fan, Y., Fisher, G.H., McClymont, A. N., 1994. Dynamics of emerging active region flux loops. ApJ 436, 907–928.

[8] Fan, Y., Gibson, S. E., 2004. Numerical simulations of three-dimensional coronal magnetic fields resulting from the emergence of twisted magnetic flux tubes. ApJ 609, 1123–1133.

[9] Fisher, G. H., Fan, Y., Howard, R. F., 1995. Comparisons between theory and observation of active region tilts. ApJ 438, 463–471.

[10] Hahn, M., Gaard, S., Jibben, P., Canfield, R. C., Nandy, D., 2005. Spatial relationship between twist in active region magnetic fields and solar flares. ApJ 629, 1135–1140.

[11] Holder, Z. A., Canfield, R. C., McMullen, R. A., Nandy, D., Howard, R. F., Pevtsov, A. A., 2004. On the tilt and twist of solar active regions. ApJ 611, 1149–1155.

[12] Hood, A.W., Priest, E.R., 1979. Kink instability of solar coronal loops as the cause of solar flares, Solar Physics, 64, 303–321.

[13] Hundhausen, A. J., 1993. Sizes and locations of coronal mass ejections - SMM observations from 1980 and 1984-1989. Journal of Geophysical Research 98, 13177–13200.

[14] Isenberg, P. A., Forbes, T. G., Demoulin, P., 1993. Catastrophic evolution of a force-free flux rope: A model for eruptive flares. ApJ 417, 368–386.

[15] Leamon, R. J., Canfield, R. C., Blehm, Z., Pevtsov, A. A., 2003. What is the role of the kink instability in solar coronal eruptions? ApJL 596, L255–L258.

[16] Leighton, R.B., 1964. Transport of magnetic fields on the sun. ApJ 140, 1547–1562.

[17] Leka, K. D., Fan, Y., Barnes, G., 2005. On the availability of sufficient twist in solar active regions to trigger the kink instability. ApJ 626, 1091–1095.

[18] Lin, J., Forbes, T. G., 2000. Effects of reconnection on the coronal mass ejection process. Journal of Geophysical Research 105, 2375–2392.

[19] Linton, M. G., Fisher, G. H., Dahlburg, R. B., Fan, Y., 1999. Relationship of the multimode kink instability to delta-Spot formation. ApJ 522, 1190–1205.

[20] Linton, M. G., Longcope, D. W., Fisher, G. H., 1996. The helical kink instability of isolated, twisted magnetic flux rubes. ApJ 469, 954–963.

[21] Low, B. C., 2001. Coronal mass ejections, magnetic flux ropes, and solar magnetism. Journal of Geophysical Research 106, 25141–25164.

[22] Mackay, D.H., Gaizauskas, G., Rickard, G.J., Priest, E.R., 1997. Force-free and potential models of a filament channel in which a filament forms. ApJ 486, 534–549.

[23] Mackay, D.H., van Ballegooijen, A.A., 2001. A possible solar cycle dependence to the hemispheric pattern of filament magnetic fields? ApJ 560, 445–455.

[24] Mackay, D.H., van Ballegooijen, A.A., 2005. New results in modeling the hemispheric pattern of solar filaments. ApJL 621, L77-L80.

[25] Mackay, D.H., van Ballegooijen, A.A., 2006a. Models of the large-scale corona. I. Formation, evolution, and liftoff of magnetic flux ropes. ApJ 641, 577–589.

[26] Mackay, D.H., van Ballegooijen, A.A., 2006b. Models of the Large-scale corona. II. Magnetic connectivity and open flux variation. ApJ 642, 1193–1204.

[27] Martin, S. F., 1998. Conditions for the formation and maintenance of filaments. Solar Physics 182, 107–137.

[28] Melville, J.P., Hood, A.W., Priest, E.R., 1986. The ideal magnetohydrodynamic stability of a line-tied coronal magnetohydrostatic equilibrium. Solar Physics 105, 291–306.

[29] Metcalf, T.R., Jiao, L., McClymont, A.N., Canfield, R.C., Uitenbroek, H., 1995. Is the solar chromospheric magnetic field force-free? ApJ 439, 474–481.

[30] Mickey, D. L., 1985. The haleakala stokes polarimeter. Solar Physics 97, 223–238.

[31] Mikić, Z., Schnack, D. D., van Hoven, G., 1990. Dynamical evolution of twisted magnetic flux tubes. I - Equilibrium and linear stability. ApJ 361, 690–700.

[32] Nandy, D., 2006. Magnetic helicity and flux tube dynamics in the solar convection zone: Comparisons between observation and theory. Journal of Geophysical Research 111, A12S01.

[33] Nandy, D., Hahn, M., Canfield, R. C., Longcope, D. W., 2003. Detection of a taylor-like plasma relaxation process in the sun. ApJL 597, L73–L76.

[34] Pevtsov, A.A., Canfield, R.C., Metcalf, T.R., 1995. Latitudinal variation of helicity of photospheric magnetic fields. ApJ 440, L109–L112.

[35] Pevtsov, A. A., 2002. Active-region filaments and x-ray sigmoids. Solar Physics 207, 111–123.

[36] Priest, E. R., 1982. Solar magneto-hydrodynamics. (Dordrecht, Holland; Boston: D. Reidel Pub. Co.; Hingham).

[37] Priest, E. R., 1989. Dynamics and structure of quiescent solar prominences. Proceedings of the Workshop, Palma de Mallorca, Spain, Nov. 1987, ASSL Vol. 150: Dynamics and Structure of Quiescent Solar Prominences.

[38] Priest, E. R., Démoulin, P., 1995. Three-dimensional magnetic reconnection without null points. 1. Basic theory of magnetic flipping. Journal of Geophysical Research 100, 23443–23464.

[39] Régnier, S., Canfield, R.C. 2006. Evolution of magnetic fields and energetics of flares in active region 8210. A&A 451, 319–330.

[40] Rust, D. M., Kumar, A., 1996. Evidence for Helically Kinked Magnetic Flux Ropes in Solar Eruptions. ApJL 464, L199–L202.

[41] Russell, C. T., Priest, E. R., Lee, L.-C., 1990. Physics of magnetic flux ropes. (Washington, D.C. : American Geophysical Union).

[42] Sammis, I., Tang, F., Zirin, H., 2000. The dependence of large flare occurrence on the magnetic structure of sunspots. ApJ 540, 583–587.

[43] Schrijver, C. J., DeRosa, M. L., Title, A. M., Metcalf, T. R., 2005. The nonpotentiality of active-region coronae and the dynamics of the photospheric magnetic field. ApJ 628, 501–513.

[44] Somov, B. V., 1992. Physical processes in solar flares. Kluwer Academic Publishers, Astrophysics and Space Science Library Vol. 172, 257.

[45] Török, T., Kliem, B., 2005. Confined and ejective eruptions of kink-unstable flux ropes. ApJL 630, L97–L100.

[46] Török, T. and Kliem, B., Titov, V.S., 2004. Ideal kink instability of a magnetic loop equilibrium. A&A 413, L27–L30.

[47] Valori, G., Kliem, B., Keppens, R. 2005. Extrapolation of a nonlinear force-free field containing a highly twisted magnetic loop. A&A 433, 335–347.

[48] van Ballegooijen, A. A., Priest, E. R., Mackay, D. H., 2000. Mean field model for the formation of filament channels on the sun. ApJ 539, 983–994.

[49] Yang, W. H., Sturrock, P. A., Antiochos, S. K., 1986. Force-free magnetic fields - The magneto-frictional method. ApJ 309, 383–391.
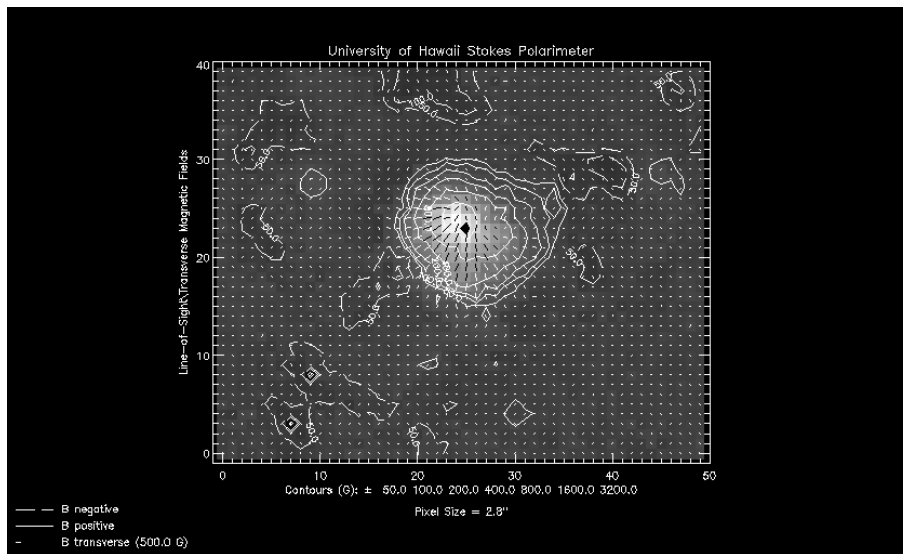
Fig. 1. Photospheric vector magnetogram of the leading polarity of the bipolar active region (Mt. Wilson β classification) AR 7289. In the background we have shown the B_z distribution (grayscale) for ease of identification of the cross-section of the inferred flux tube. Positive and negative vertical magnetic field contours are depicted in solid and dashed lines respectively and short white arrows depict transverse field vectors. The derived location of the FWC is indicated by a black diamond.
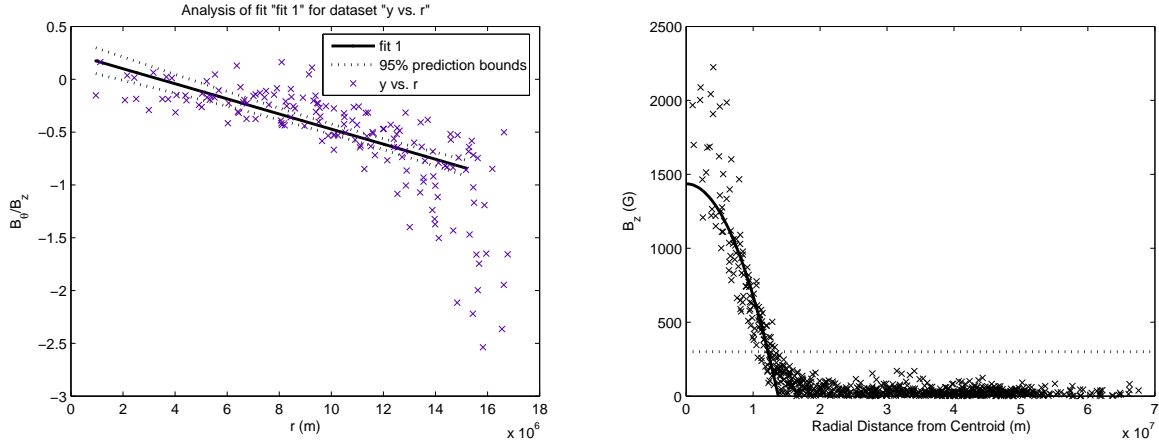
Fig. 2. Left: A plot of the B_θ/B_z versus radial distance r distribution for AR 7289 – from which we extract the best-fit slope to quantify the overall twist q_{fit} following techniques described in Section 2. The solid line shows the fit, while the dotted lines indicate the 95% confidence bounds. The recovered best-fit twist $q_{fit} = -4.89 \times 10^{-8}$ m^{-1}. Only those magnetogram pixels that are over specified noise thresholds are used for the calculation. Right: Axial (vertical) field B_z versus radial distance r distribution for AR 7289 – to which we fit Equation 4 as described in Section 2. The recovered fit parameters are B_0 and μ which we use to plot the best-fit curve (solid line). The inferred critical twist $q_{crit} = \mu^{1/2} = -7.27 \times 10^{-8}$ m^{-1}. Although we show the radial profile of B_z over the whole magnetogram here, note that only B_z values over a threshold of 300 G (dotted line) have been used in the determination of q_{crit} (see text).
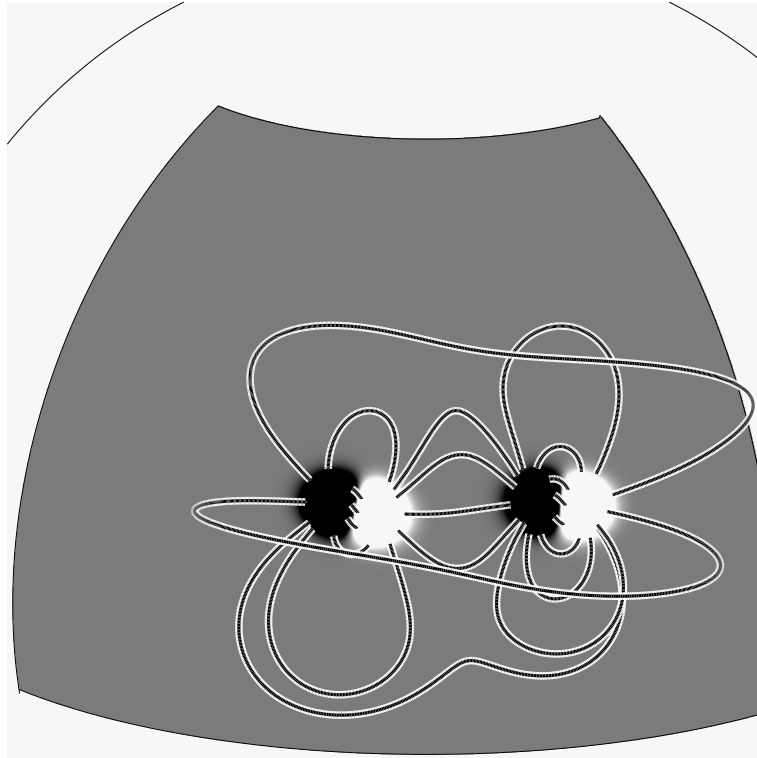
Fig. 3. (a) Initial magnetic field distribution when the bipoles are inserted and the coronal field relaxes to equilibrium. The simulations is carried out mainly in the Northern Hemisphere.
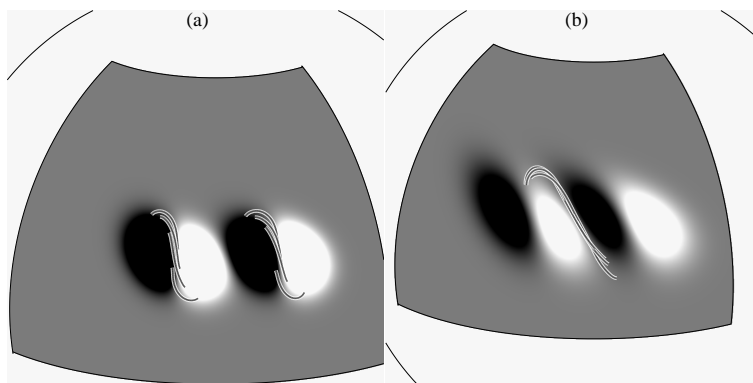

Fig. 4. Example of the inverse S-shaped (sigmoidal) flux ropes formed over (a) the two internal PIL on day 20, (b) the external PIL between the bipoles on day 45.
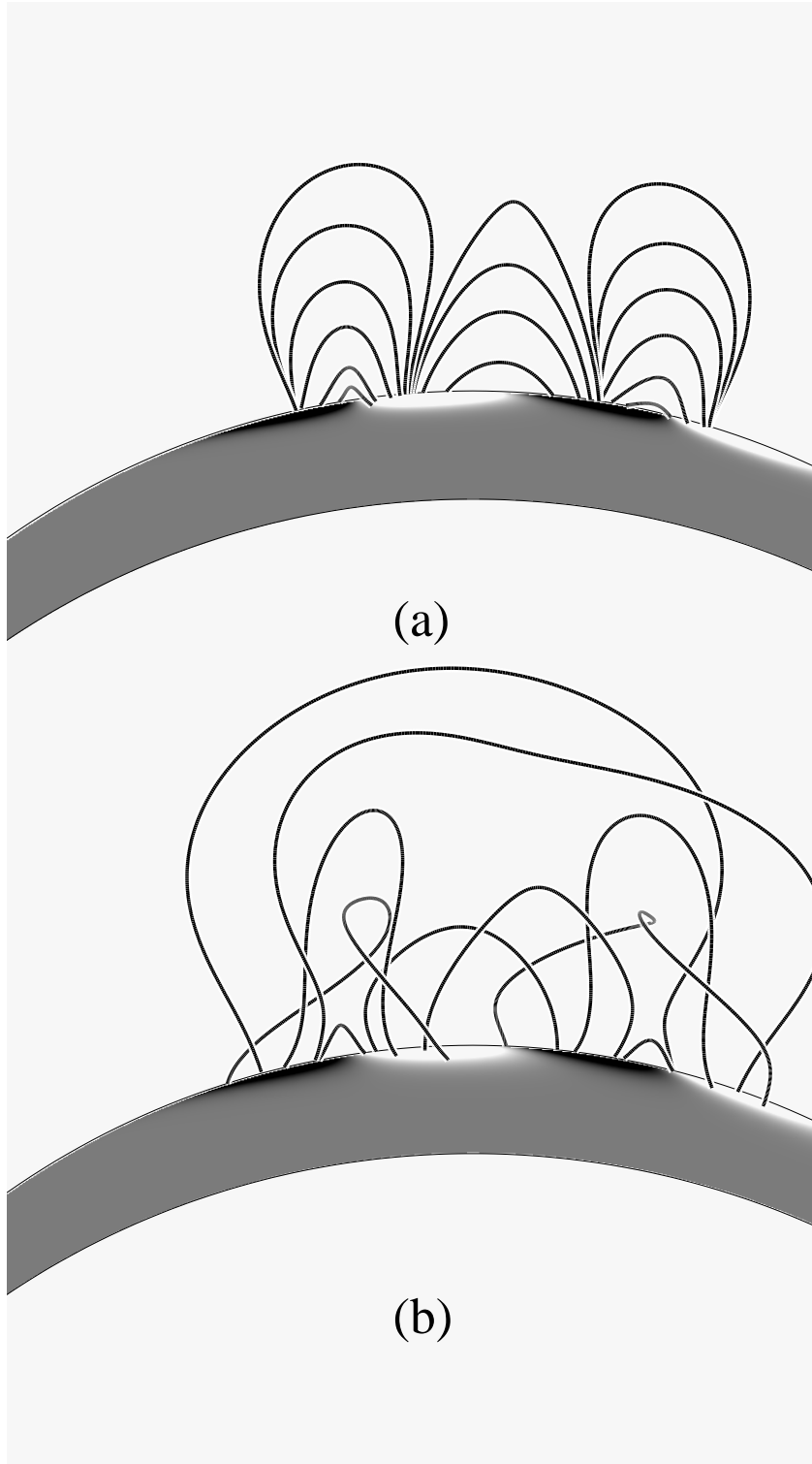
Fig. 5. Example of the simultaneous lift off of the flux ropes lying above the internal PILs of both bipoles on (a) day 20, (b) day 30. In (b) the formation of a quasi-separatrix layer occurs below each flux rope in the form of an X-line when viewed in 2D. This quasi-separatrix layers are seen to rise as the flux ropes rise.